DOI: 10.1002/adem.200900130

Heat-Transfer Coefficient for Cellular Materials Modelled as an Array of Elliptic Rods**

By *Marcelo J. S. de Lemos** and *Marcelo B. Saito*

This work deals with the numerical determination of the interfacial heat-transfer coefficient in cellular materials, in which the solid structure is modelled as an ordered array of elliptic rods. The cases herein studied concern those in which the average temperatures for the fluid and the solid matrix differ substantially, in a way that the local-thermal-equilibrium hypothesis (LTE) is no longer valid.[1–4] The local-thermal-non-equilibrium hypothesis (LTNE) is employed in order to obtain the average temperatures for the fluid and solid phases.[5–6]

Accordingly, a numerical procedure to determine the macroscopic transport coefficients from a theoretical basis was first proposed by Kuwahara et al.[7] They used a single unit cell and determined the interfacial heat-transfer coefficient for the asymptotic case of infinite conductivity of the solid phase. Nakayama et al.[8] extended the conduction model of Hsu[9] for also treating convection in porous media. Further, forced convection in porous media is fully documented in ref. [3,10,11] Having established the macroscopic energy equations for both phases, useful exact solutions were obtained for two fundamental heat-transfer processes associated with porous media, namely, steady conduction in a porous slab with internal heat generation within the solid, and also for a thermally developing flow through a semi-infinite porous medium. Saito and de Lemos[12] considered local thermal non-equilibrium and obtained the interfacial heat-transfer coefficient for laminar flow using a single unit cell with local instantaneous transport equations. Although only laminar flow was considered in all of the studies mentioned above, turbulent flow needs also to be investigated due to the number of practical applications in which the fluid undergoes a transition towards the turbulent regime.

When treating turbulent flow in porous media, however, difficulties arise due to the fact that the flow fluctuates with time, a volumetric average being applied.[13] For handling such situations, a new concept called double decomposition has been proposed for developing macroscopic models for turbulent transport in porous media.[14,15] This methodology has been extended to nonbuoyant heat transfer under local thermal equilibrium,[16,17] buoyant flows,[18–22] mass transfer[23] and double diffusion,[24] including applications in channels with porous baffles[25,26] and impinging jets.[27] In addition, a general classification of models has been published.[28] Recently, the problem of treating interfaces between a finite porous medium and free flow, considering a diffusion-jump condition for laminar[29] and turbulent regime,[30,31] has also been investigated under the concept first presented by Pedras and de Lemos.[14,15] Following this same concept, Saito and de Lemos[32] proposed a new correlation for obtaining the interfacial heat-transfer coefficient for turbulent flow in a packed bed in which the porous material was modelled as an infinite staggered array of square rods. Recently, an extension of the analysis therein to moving porous beds has been published.[33,34]

This work focuses on turbulent flow through a foam-like material, which represents an important configuration for efficient heat transfer and suggests the use of equations governing the energy balances for both the solid and fluid phases. Accordingly, the use of such a two-energy-equation model requires the heat-transfer coefficient between the phases.

Therefore, the problem here comprises calculating such a convective heat-transfer coefficient for laminar and turbulent flow in cellular materials, which are modelled considering an infinite array of elliptic rods. The range of the Reynolds number (Re_D), based on the hydraulic diameter of the rod, is varied from the laminar regime up to 10^7.

Macroscopic Governing Equations

Macroscopic transport equations for turbulent flow in a porous medium are obtained through the simultaneous application of time- and volume-average operators, resulting in Equation (1), wherein $\overline{\mathbf{u}}_D = \phi\langle\overline{\mathbf{u}}\rangle^{\mathrm{i}}$ and $\langle\overline{\mathbf{u}}\rangle^{\mathrm{i}}$ identifies the intrinsic (liquid) average of the time-averaged velocity vector, $\overline{\mathbf{u}}$.

$$\text{Continuity}: \nabla\cdot\overline{\mathbf{u}}_D = 0 \tag{1}$$

The momentum transport equation is described by Equation (2), where the last two terms represent the Darcy and Forchheimer contributions:[35]

$$\rho\left[\frac{\partial\overline{\mathbf{u}}_D}{\partial t} + \nabla\cdot\left(\frac{\overline{\mathbf{u}}_D\overline{\mathbf{u}}_D}{\phi}\right)\right] = -\nabla(\phi\langle\overline{p}\rangle^{\mathrm{i}}) + \mu\nabla^2\overline{\mathbf{u}}_D - \nabla\cdot(\rho\phi\langle\overline{\mathbf{u}'\mathbf{u}'}\rangle^{\mathrm{i}}) - \left[\frac{\mu\phi}{K}\overline{\mathbf{u}}_D + \frac{c_{\mathrm{F}}\phi\rho|\overline{\mathbf{u}}_D|\overline{\mathbf{u}}_D}{\sqrt{K}}\right] \tag{2}$$

[*] *M. J. S. de Lemos, M. B. Saito*
Departamento de Energia, IEME, Instituto Tecnológico de Aeronáutica (ITA)
12228-900, São José dos Campos, SP, Brazil
E-mail: delemos@ita.br

[**] *The authors are thankful to CNPq and FAPESP, Brazil, for their invaluable financial support during the course of this research.*

COMMUNICATION

In Equation (2), the symbol K is the porous medium permeability; c_F is the form-drag or Forchheimer coefficient; $\langle\overline{p}\rangle^i$ is the intrinsic average pressure of the fluid and ϕ is the porosity of the porous medium. The macroscopic Reynolds stress, $-\rho\phi\langle\overline{\mathbf{u}'\mathbf{u}'}\rangle^i$, appearing in Equation (2) is given by Equation (3):

$$-\rho\phi\langle\overline{\mathbf{u}'\mathbf{u}'}\rangle^i = \mu_{t_\phi} 2\langle\overline{\mathbf{D}}\rangle^v - \frac{2}{3}\phi\rho\langle k\rangle^i\mathbf{I} \tag{3}$$

In Equation (3):

$$\langle\overline{\mathbf{D}}\rangle^v = \frac{1}{2}\left[\nabla(\phi\langle\overline{\mathbf{u}}\rangle^i) + [\nabla(\phi\langle\overline{\mathbf{u}}\rangle^i)]^T\right] \tag{4}$$

$\langle\overline{\mathbf{D}}\rangle^v$ is the macroscopic deformation tensor, $\langle k\rangle^i = \langle\overline{\mathbf{u}'\cdot\mathbf{u}'}\rangle^i/2$ is the intrinsic turbulent kinetic energy, and μ_{t_ϕ}, is the turbulent viscosity, which is modelled in ref. [28] similarly to the case of clear flow, in the form described in Equation (5):

$$\mu_{t_\phi} = \rho c_\mu \frac{\langle k\rangle^{i2}}{\langle\varepsilon\rangle^i} \tag{5}$$

The intrinsic turbulent kinetic energy per unit mass and its dissipation rate are governed by Equation (6) and (7), in which c_1 and c_2 are constants:

$$\rho\left[\frac{\partial}{\partial t}\left(\phi\langle k\rangle^i\right) + \nabla\cdot\left(\overline{\mathbf{u}}_D\langle k\rangle^i\right)\right] = \nabla\cdot\left[\left(\mu + \frac{\mu_{t_\phi}}{\sigma_k}\right)\nabla\left(\phi\langle k\rangle^i\right)\right] - \rho\langle\overline{\mathbf{u}'\mathbf{u}'}\rangle^i : \nabla\overline{\mathbf{u}}_D + c_k\rho\frac{\phi\langle k\rangle^i|\overline{\mathbf{u}}_D|}{\sqrt{K}} - \rho\phi\langle\varepsilon\rangle^i \tag{6}$$

$$\rho\left[\frac{\partial}{\partial t}\left(\phi\langle\varepsilon\rangle^i\right) + \nabla\cdot\left(\overline{\mathbf{u}}_D\langle\varepsilon\rangle^i\right)\right] = \nabla\cdot\left[\left(\mu + \frac{\mu_{t_\phi}}{\sigma_\varepsilon}\right)\nabla\left(\phi\langle\varepsilon\rangle^i\right)\right] + c_1\left(-\rho\langle\overline{\mathbf{u}'\mathbf{u}'}\rangle^i : \nabla\overline{\mathbf{u}}_D\right)\frac{\langle\varepsilon\rangle^i}{\langle k\rangle^i} + c_2c_k\rho\frac{\phi\langle\varepsilon\rangle^i|\overline{\mathbf{u}}_D|}{\sqrt{K}} - c_2\rho\phi\frac{\langle\varepsilon\rangle^{i2}}{\langle k\rangle^i} \tag{7}$$

Similarly, macroscopic energy equations are obtained for both the fluid and solid phases by applying time- and volume-average operators to the instantaneous local equations. As in the flow case, volume integration is performed over a representative elementary volume (REV), resulting in Equation (8) and (9):

$$\left\{\left(\rho c_p\right)_f\phi\right\}\frac{\partial\langle\overline{T}\rangle^i}{\partial t} + \left(\rho c_p\right)_f\nabla\cdot\left(\mathbf{u}_D\langle\overline{T_f}\rangle^i\right) = \nabla\cdot\left\{\mathbf{K}_{eff,f}\cdot\nabla\langle\overline{T}_f\rangle^i\right\} + h_ia_i\left(\langle\overline{T_s}\rangle^i - \langle\overline{T_f}\rangle^i\right) \tag{8}$$

$$\left\{(1-\phi)\left(\rho c_p\right)_s\right\}\frac{\partial\langle\overline{T}\rangle^i}{\partial t} = \nabla\cdot\left\{\mathbf{K}_{eff,s}\cdot\nabla\langle\overline{T_s}\rangle^i\right\} - h_ia_i\left(\langle\overline{T_s}\rangle^i - \langle\overline{T_f}\rangle^i\right) \tag{9}$$

In Equation (8) and (9), $\mathbf{K}_{eff,f}$ and $\mathbf{K}_{eff,s}$ are the effective conductivity tensors for the fluid and solid, respectively, and $a_i = A_i/\Delta V$ is the interfacial area per unit volume. The tensors are given by Equation (10) and Equation (11), respectively, wherein $\mathbf{I}$ is the unit tensor (see ref. [32] for details):

$$\mathbf{K}_{eff,f} = [\phi k_f]\mathbf{I} + \mathbf{K}_{f,s} + \mathbf{K}_t + \mathbf{K}_{disp} + \mathbf{K}_{disp,t} \tag{10}$$

$$\mathbf{K}_{eff,s} = [(1-\phi)k_s]\mathbf{I} + \mathbf{K}_{s,f} \tag{11}$$

Interfacial Heat-Transfer Coefficient, h_i

In Equation (8) and (9), the heat transferred between the two phases was modelled by means of a film coefficient, h_i. For a staggered configuration of tube banks, Žukauskas[36] proposed the following correlation (Equation (12)) for it, where the values 0.022 and 0.84 are for tubes in cross flow:

$$\frac{h_iD}{k_f} = 0.022Re_D^{0.84}Pr^{0.36}, \text{for } 2\times10^5 < \mathrm{Re}_D < 2\times10^6 \tag{12}$$

Wakao et al.[37] obtained a heuristic correlation for a closely packed bed with particle diameter D and compared their results with experimental data. This correlation for the interfacial heat-transfer coefficient is given by Equation (13):

$$\frac{h_iD}{k_f} = 2 + 1.1Re_D^{0.6}Pr^{1/3} \tag{13}$$

For determining h_i numerically, Kuwahara et al.[7] and Nakayama et al.[8] modelled porous media by considering the medium as being an infinite number of solid, square rods of size D, arranged in a regular triangular pattern. They numerically solved the governing equations in the void region, exploiting the fact that, for an infinite and geometrically ordered medium, a repetitive cell can be identified. Periodic boundary conditions were then applied for obtaining the temperature distribution under fully developed flow conditions. A numerical correlation for the interfacial convective heat-transfer coefficient was proposed by Kuwahara et al.[7] for laminar flow as shown in Equation (14):

$$\frac{h_iD}{k_f} = \left(1 + \frac{4(1-\phi)}{\phi}\right) + \frac{1}{2}(1-\phi)^{1/2}\mathrm{Re}_D\,\mathrm{Pr}^{1/3}, \quad \text{valid for } 0.2 < \phi < 0.9 \tag{14}$$

In this way, the macroscopic behavior of permeable media can be obtained by integrating the distributed parameters obtained at the pore scale. If we consider the medium to be infinite and orderly arranged, a single structural unit may be identified and taken as the calculation domain (Fig. 1a). Computations within this cell were carried out using a non-uniform grid (Fig. 1b). The Reynolds number, $Re_D = \rho\overline{\mathbf{u}}_DD/\mu$, was varied from 10^4 to 10^7

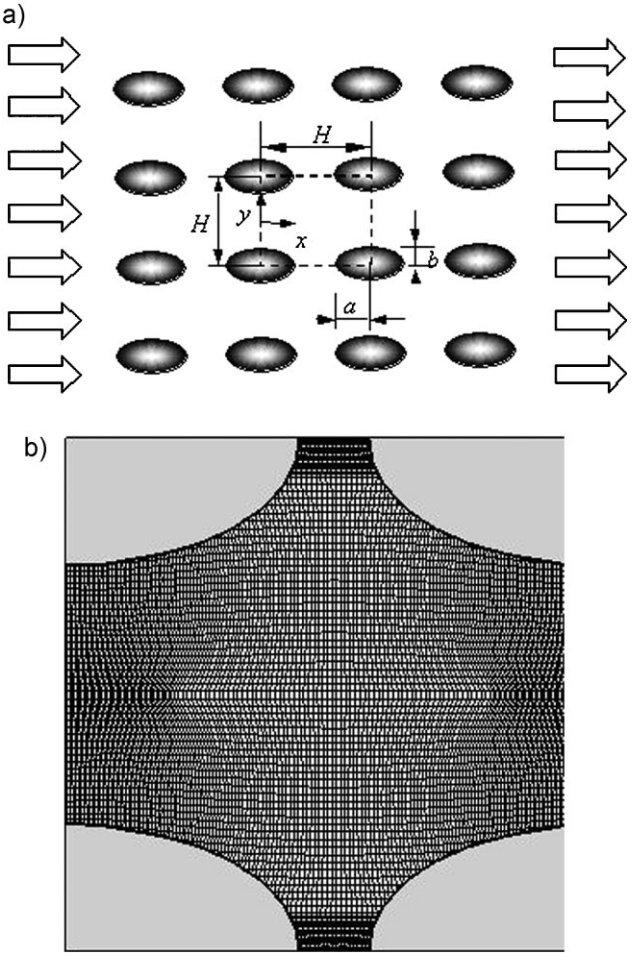

Fig. 1. a) Physical model and coordinate system. b) Non-uniform computational grid.

where $D = 2ab(a^2 + b^2)^{-0.5}$. The cell porosity is given by $\phi = 1 - (D/H)^2$.

The boundary and periodic conditions are as follows:

On solid walls (laminar or low *Re* number model):

$$\overline{u} = 0,\ k = 0,\ \varepsilon = \nu\frac{\partial^2 k}{\partial y^2},\ \overline{T} = \overline{T}_{\mathrm{w}} \tag{15}$$

On solid walls (high *Re* model):

$$\frac{\overline{u}}{u_\tau} = \frac{1}{\kappa}\ln(y^+E),\ k = \frac{u_\tau^2}{{c_\mu}^{1/2}},\ \varepsilon = \frac{{c_\mu}^{3/4}k_{\mathrm{w}}^{3/2}}{\kappa y_{\mathrm{w}}},$$
$$q_{\mathrm{w}} = \frac{(\rho c_{\mathrm{p}})_{\mathrm{f}}{c_\mu}^{1/4}k_{\mathrm{w}}^{1/2}(\overline{T} - T_{\mathrm{w}})}{\left(\frac{\sigma_{\mathrm{t}}}{\kappa}\ln(y_{\mathrm{w}}^+) + c_Q(Pr)\right)} \tag{16}$$

In Equation (16), $u_\tau = \left(\frac{\tau_{\mathrm{w}}}{\rho}\right)^{1/2}$, $y_{\mathrm{w}}^+ = \frac{y_{\mathrm{w}}u_\tau}{\nu}$, and $c_Q = 12.5Pr^{2/3} + 2.12\ln(Pr) - 5.3$ for $Pr > 0.5$

In Equation (16), Pr and σ_{t} are the Prandtl and turbulent Prandtl numbers, respectively, q_{w} is the wall heat flux, u_τ is the wall-friction velocity, y_{w} is the coordinate normal to the wall and κ is the von Kármán constant. Furthermore, in Equation (16), E is equal to 9.0 for smooth walls. The other boundary conditions are:

On the symmetry planes:

$$\frac{\partial\overline{u}}{\partial y} = \frac{\partial k}{\partial y} = \frac{\partial\varepsilon}{\partial y} = 0 \tag{17}$$

On the periodic boundaries:

$$\overline{u}|_{\mathrm{inlet}} = \overline{u}|_{\mathrm{outlet}},\ \overline{v}|_{\mathrm{inlet}} = \overline{v}|_{\mathrm{outlet}},\ k|_{\mathrm{inlet}} = k|_{\mathrm{outlet}},\ \varepsilon|_{\mathrm{inlet}} = \varepsilon|_{\mathrm{outlet}} \tag{18}$$

$$\theta|_{\mathrm{inlet}} = \theta|_{\mathrm{outlet}} \Leftrightarrow \left.\frac{\overline{T} - \overline{T}_{\mathrm{w}}}{\overline{T}_{\mathrm{B}}(x) - \overline{T}_{\mathrm{w}}}\right|_{\mathrm{inlet}} = \left.\frac{\overline{T} - \overline{T}_{\mathrm{w}}}{\overline{T}_{\mathrm{B}}(x) - \overline{T}_{\mathrm{w}}}\right|_{\mathrm{outlet}} \tag{19}$$

The bulk mean temperature of the fluid is given by Equation (20):

$$\overline{T}_{\mathrm{B}}(x) = \frac{\int\overline{u}\overline{T}dy}{\int\overline{u}dy} \tag{20}$$

Computations are based on the Darcy velocity, the length of structural unit, H, and the temperature difference $\left(\overline{T}_{\mathrm{B}}(x) - \overline{T}_{\mathrm{w}}\right)$, as reference scales.

Determination of h_{i} is here obtained by calculating, for the unit cell of Figure 1a, an expression given by Equation (21) where $A_{\mathrm{i}} = 2\pi\left(0.5\left(a^2 + b^2\right)\right)^{0.5}$:

$$h_{\mathrm{i}} = \frac{Q_{\mathrm{total}}}{A_{\mathrm{i}}\Delta T_{\mathrm{ml}}} \tag{21}$$

The overall heat transferred in the cell, Q_{total}, is given by Equation (22):

$$Q_{\mathrm{total}} = (H - 2b)\rho\overline{u}_{\mathrm{B}}c_{\mathrm{p}}\left(\overline{T}_{\mathrm{B}}\big|_{\mathrm{outlet}} - \overline{T}_{\mathrm{B}}\big|_{\mathrm{inlet}}\right), \tag{22}$$

The bulk mean velocity of the fluid is given by Equation (23):

$$\overline{u}_{\mathrm{B}}(x) = \frac{\int\overline{u}dy}{\int dy} \tag{23}$$

The logarithm mean temperature difference, ΔT_{ml} is given by Equation (24):

$$\Delta T_{\mathrm{ml}} = \frac{\left(\overline{T}_{\mathrm{w}} - \overline{T}_{\mathrm{B}}\big|_{\mathrm{outlet}}\right) - \left(\overline{T}_{\mathrm{w}} - \overline{T}_{\mathrm{B}}\big|_{\mathrm{inlet}}\right)}{\ln\left[\left(\overline{T}_{\mathrm{w}} - \overline{T}_{\mathrm{B}}\big|_{\mathrm{outlet}}\right)\left(\overline{T}_{\mathrm{w}} - \overline{T}_{\mathrm{B}}\big|_{\mathrm{inlet}}\right)\right]} \tag{24}$$

Equation (22) represents the overall heat balance over the entire cell and considers the heat transferred to the fluid to be associated to a suitable temperature difference, ΔT_{ml}. The local instantaneous equations were numerically solved in the unit cell until conditions given by Equation (18) and Equation (19) were satisfied.

Results and Discussion

Figure 2 compares integrated h_{i} values for square and elliptic rods, for porosities $\phi = 0.75$ and $\phi = 0.90$, covering the laminar-flow range $3.5 \leq Re_D \leq 350$. Also shown are results by Kuwahara et al.[7] It is interesting to note that the more

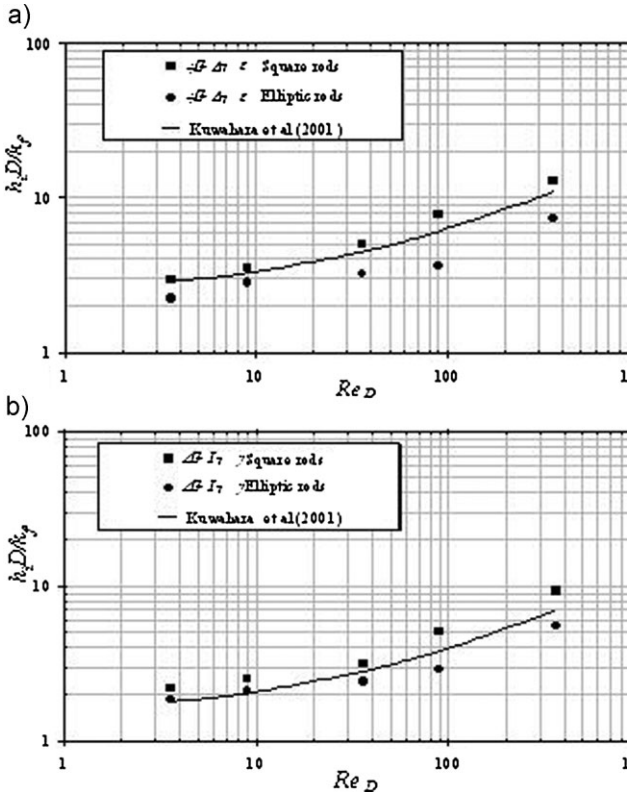

Fig. 2. a) Comparison between square rods, elliptic rods and correlation of Kuwahara et al.[7] for $\phi = 0.75$. b) Comparison between square rods, elliptic rods and correlation of Kuwahara et al.[7] $\phi = 0.90$.

streamlined the flow is, over the elliptic rods displaced in an aligned manner, the less its effectiveness in promoting heat transfer between the phases. Furthermore, the higher the Re_D number, the higher the heat-transfer coefficient. Figure 3 compiles h_i values as a function of the porosity ϕ for Re_D up to 1000. In this case, the lower the porosity, the higher the heat-transfer rate for the same mass-flow rate across the bed (same Re_D). In addition, as Re_D increases, the effect of ϕ on h_i becomes less pronounced. Also, the Figure seems to indicate two distinct regimes, the first one for $Re_D < 100$ and the second for $Re_D > 100$. However, the limited amount of data presented here does not allow more-definite conclusions to be drawn.

Results for high Re numbers are shown next. Figure 4 shows the distributions of the pressure, turbulence kinetic energy and temperature fields in the periodic cell considered in Figure 1, which were obtained for $Re_D = 10^5$ and for $\phi = 0.60$ and $\phi = 0.90$. One can observe that the pressure increases at the left face of the rod and decreases behind it (Figure 4a–b), with the surface peak pressure moving towards the stagnation point on the left, along the ellipses' horizontal axes, as ϕ increases. The turbulence-kinetic-energy distribution is shown in Figure 4c–d. Levels of k are higher close to the walls and along the converging section of the channel, where a strong shear layer prevails. The temperature-distribution pattern is shown in Figure 4e–f, showing that a thermal boundary layer covers most of the surface, possibly indicating

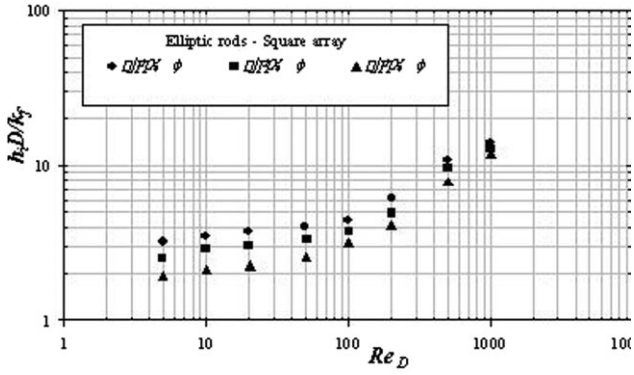

Fig. 3. Effect of porosity on h_i for $Pr = 1$ and laminar flow.

that convective heat transfer surpasses thermal diffusion for the case of high mass-flow rates.

Results for $h_i D/k_f$ are plotted in Figure 5 for Re_D up to 10^7. Also plotted are computations using Correlation (14) by Kuwahara et al.[7] for the case of $\phi = 0.65$. The figure seems to indicate that the present computations show a reasonable agreement for laminar flow. For comparison, numerical results for turbulent flow using low and high Re models are also presented in this Figure ($10^3 < Re_D < 10^4$). Differences in the flow pattern caused by distinct obstacle arrangements, namely, the aligned elliptic rods and staggered square obstacles, are reflected in the lower heat-transfer coefficients for the former case. The sharp edges of the square obstacles, disposed in a triangular arrangement, agitate the fluid in a much stronger way that in the case of a streamlined flow across elliptic tubes.

Figure 6 shows the numerical results for the interfacial convective heat-transfer coefficient for porosities $\phi = 0.65$ and $\phi = 0.90$. Results for $h_i D/k_f$ are plotted for Re_D up to 10^7, comparing the two geometries analyzed here. The lower the porosity, the higher the $h_i D/k_f$ ratio: this is an effect that is much less pronounced when computing the more-clear flow past the inline-arranged elliptic rods.

For square-rod arrays in the staggered arrangement, the numerical correlation for the interfacial heat-transfer coefficient proposed by Kuwahara et al.[7] was set for laminar flow only, whereas for turbulent flow another correlation by Saito and de Lemos[32] has been proposed. The results herein, which consider elliptic rods instead, can be used in developing more-complex correlations that will eventually take into account the rod shape and the array layout. As such, the results herein can be seen as a step contributing towards such a goal.

Conclusions

Turbulent flow through a cellular (foam-like) material modelled as an array of elliptic rods is analyzed. Details are presented for determining the convective heat-exchange coefficient between the porous substrate and the working fluid. Results for turbulent flow through a periodic cell of isothermal elliptic rods were computed, considering periodic boundary conditions for the velocity and temperature fields.

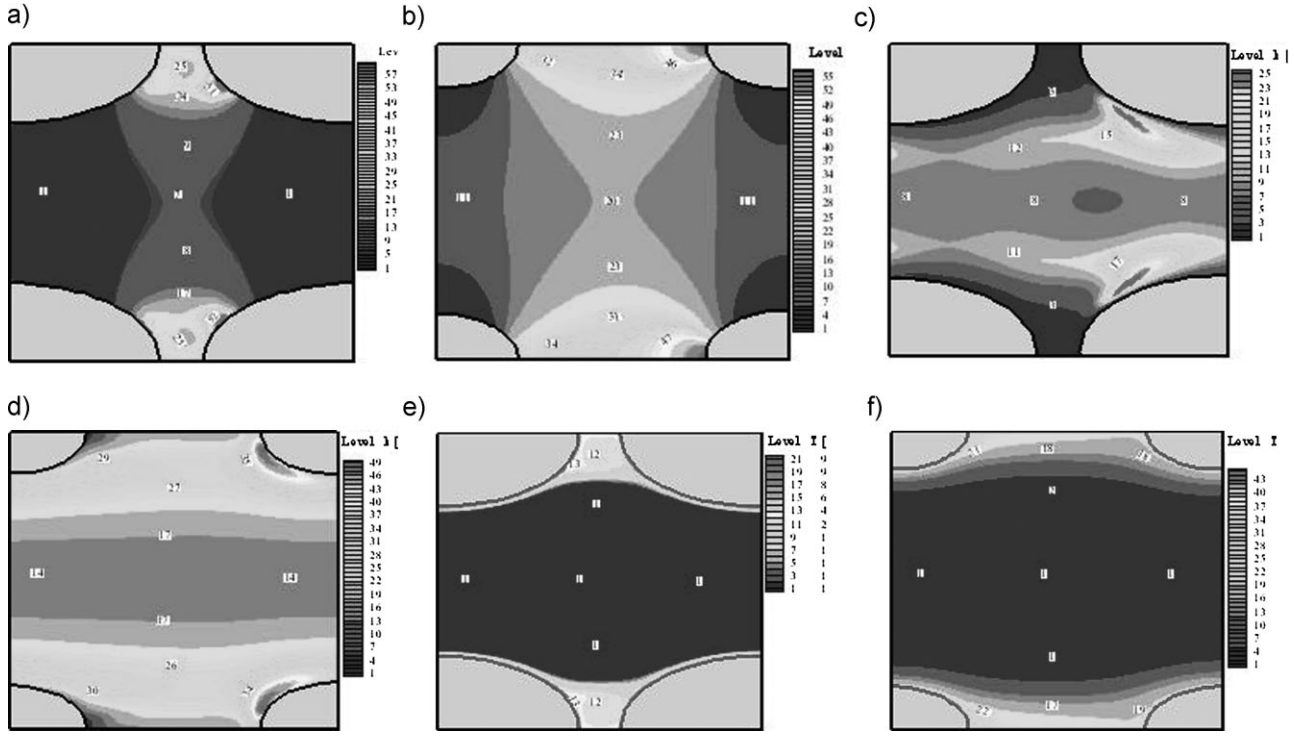

Fig. 4. Elliptic rods for $Re_D = 1 \times 10^5$: a) non-dimensional pressure for $\phi = 0.65$; b) non-dimensional pressure for $\phi = 0.90$; c) turbulence kinetic energy for $\phi = 0.65$; d) turbulence kinetic energy for $\phi = 0.90$; e) temperature field for $\phi = 0.65$; f) temperature field for $\phi = 0.90$.

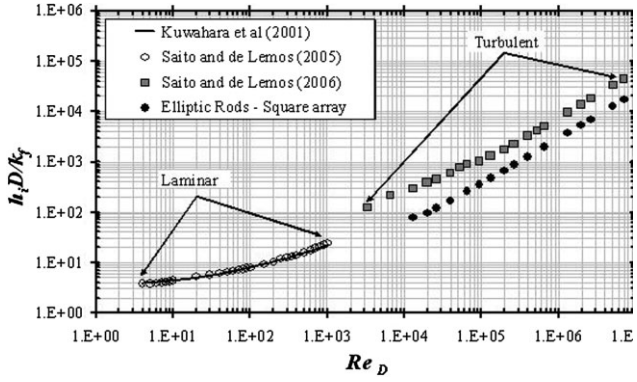

Fig. 5. Effect of Re_D on h_i for $Pr = 1$ and $\phi = 0.65$ and turbulent flow.

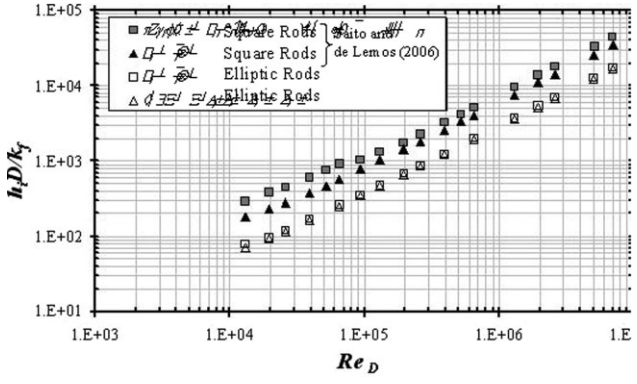

Fig. 6. Effect of Re_D on h_i for various porosities and different shapes.

For turbulent flows, low and high Reynolds turbulence models were employed in order to obtain the interfacial heat-transfer coefficient. The results indicate that, for the same mass-flow rate, materials that resemble or that can be modelled as arrays of elliptic rods present a lower interfacial heat-transfer coefficient when compared to other media modelled as staggered arrays of square rods. Additional work will be carried out in order to simulate fully turbulent flow and heat transfer in a porous medium formed by arrays of elliptical rods displaced in both ''in-line'' and ''staggered'' arrangements. Finally, it is expected that a more-general correlation for h_i can be obtained, to be used in conjunction with macroscopic two-energy-equation models.

Nomenclature

A_i	Interface total area between the fluid and solid
c_F	Forchheimer coefficient
c_p	Fluid specific heat
D	Hydraulic diameter
h_i	Interfacial convective heat-transfer coefficient
H	Periodic cell height
$\mathbf{I}$	Unit tensor
K	Permeability
k	Turbulence kinetic energy per unit mass
k_f	Fluid thermal conductivity
k_s	Solid thermal conductivity
$\mathbf{K}_{disp}$	Dispersion conductivity tensor
$\mathbf{K}_{f,s}$	Two-equation model effective thermal conductivity tensor in fluid phase.

$\mathbf{K}_{s,f}$	Two-equation model effective thermal conductivity tensor in solid phase.
$\mathbf{K}_t$	Turbulence conductivity tensor
$\mathbf{K}_{disp,t}$	Turbulent dispersion tensor
P	Pressure
P^*	$P^* = \frac{P-P_{min}}{P_{max}-P_{min}}$: Non-dimensional Pressure
Pr	$Pr = \nu/\alpha$, Prandtl number
Re_D	Reynolds number based on D and the macroscopically uniform velocity
T	Temperature
$\overline{T}$	Time-averaged temperature
$\mathbf{u}$	Microscopic velocity
$\mathbf{u}_D$	Darcy or superficial velocity (volume average of $\mathbf{u}$)
α	Fluid thermal diffusivity
ΔV	Representative elementary volume
ΔV_f	Fluid volume inside ΔV
μ	Fluid dynamic viscosity
μ_t	Eddy viscosity
μ_{t_ϕ}	Macroscopic eddy viscosity
ν	Fluid kinematic viscosity
ρ	Fluid density
ϕ	$\phi = \Delta V_f/\Delta V$, Porosity
θ	$\theta = \frac{T-T_w}{T_B-T_w}$, Dimensionless temperature.

Received: May 13, 2009
Final Version: June 2, 2009
Published online: September 1, 2009

[1] T. E. W. Schumann, *J. Franklin. Inst.* **1929**, *208*, 405.
[2] M. Quintard, in *Proc. 11th Int. Heat-Transfer Conf* Kyongyu, Korea, J. S. Lee (Ed.), Vol. 1, Taylor and Francis, Philadelphia **1998**, 279–285.
[3] D. B. Ingham, I. Pop, *Transport Phenomena in Porous Media*, Elsevier, Amsterdam **1998**, 103–129
[4] M. Kaviany, *Principles of Heat Transfer in Porous Media*, 2nd ed. Springer, New York **1995**.
[5] M. Quintard, M. Kaviany, S. Whitaker, *Adv. Water Resources* **1997**, *20*, 77.
[6] J. A. Ochoa-Tapia, S. Whitaker, *Int. J. Heat Mass Transfer* **1997**, *40*, 2691.
[7] F. Kuwahara, M. Shirota, A. Nakayama, *Int. J. Heat Mass Transfer* **2001**, *44*, 1153.
[8] A. Nakayama, F. Kuwahara, M. Sugiyama, G. Xu, *Int. J. Heat Mass Transfer.* **2001**, *44*, 4375.
[9] C. T. Hsu, *J. Heat Transfer* **1999**, *121*, 733.
[10] D. A. Nield, A. Bejan, *Convection in Porous Media*, Springer, New York **1992**.
[11] J. Bear, *Dynamics of Fluids in Porous Media*, American Elsevier Pub. Co, New York **1972**.
[12] M. B. Saito, M. J. S. de Lemos, *Int. Comm. Heat Mass Transfer* **2005**, *32*, 666.
[13] W. G. Gray, P. C. Y. Lee, *Int. J. Multiphase Flow* **1977**, *3*, 333.
[14] M. H. J. Pedras, M. J. S. de Lemos, *Int. Comm. Heat Mass Transfer* **2000**, *27*, 211.
[15] M. H. J. Pedras, M. J. S. de Lemos, *Numer. Heat Transfer, Part A: Appl.* **2003**, *43*, 585.
[16] F. D. Rocamora, Jr, M. J. S. de Lemos, *Int. Comm. Heat Mass Transfer* **2000**, *27*, 825.
[17] M. J. S. de Lemos, F. D. Rocamora, in *Proceedings of the Twelfth International Heat-Transfer Conference* Grenoble, France, August 18-23, J. Taine (Ed.), Vol. 2, Elsevier, Amsterdam **2002**, pp. 791–796.
[18] M. J. S. de Lemos, E. J. Braga, *Int. Comm. Heat Mass Transfer* **2003**, *30*, 615.
[19] E. J. Braga, M. J. S. de Lemos, *Int. J. Heat Mass Transfer* **2004**, *47*, 5639.
[20] E. J. Braga, M. J. S. de Lemos, *Int. J. Heat Mass Transfer* **2005**, *48*, 4748.
[21] E. J. Braga, M. J. S. de Lemos, *Int. Comm. Heat Mass Transfer* **2005**, *32*, 1289.
[22] E. J. Braga, M. J. S. de Lemos, *J Heat Transfer* **2006**, *128*, 1122.
[23] M. J. S. de Lemos, M. S. Mesquita, *Int. Comm. Heat Mass Transfer* **2003**, *30*, 105.
[24] M. J. S. de Lemos, L. A. Tofaneli, *Int. J. Heat Mass Transfer* **2004**, *47*, 4233.
[25] M. Assato, M. H. J. Pedras, M. J. S. de Lemos, *J. Porous Media* **2005**, *8*, 13.
[26] N. B. Santos, M. J. S. de Lemos, *Numer. Heat Transfer, Part A: Appl.* **2006**, *49*, 546.
[27] D. R. Graminho, M. J. S. de Lemos, *Numer. Heat Transfer, Part A: Appl.* **2008**, *54*, 151.
[28] M. J. S. de Lemos, M. H. J. Pedras, *J. Fluids Eng.* **2001**, *123*, 935.
[29] R. A. Silva, M. J. S. de Lemos, *Numer. Heat Transfer, Part A: Appl.* **2003**, *43*, 603.
[30] M. J. S. de Lemos, *Int. Comm. Heat Mass Transfer* **2005**, *32*, 107.
[31] M. J. S. de Lemos, R. A. Silva, *Int. J. Heat Mass Transfer* **2006**, *49*, 546.
[32] M. B. Saito, M. J. S. de Lemos, *J. Heat Transfer* **2006**, *128*, 444.
[33] M. J. S. de Lemos, *Acta Geophysica* **2008**, *56*, 562.
[34] M. J. S. de Lemos, *Int. Comm. Heat Mass Transfer* **2008**, *35*, 1049.
[35] P. Forchheimer, *Z. Vereines Deutscher Ingenieure* **1901**, *45*, 1782.
[36] A. Žukauskas, *in Advances in Heat Transfer*, Volume, *8*, (Eds: J. P. Hartnett, T. F. Irvine Jr) Academic Press, New York **1972**, pp. 93–160.
[37] N. Wakao, S. Kaguei, T. Funazkri, *Chem. Eng. Sci.* **1979**, *34*, 325.

